Enhanced properties of PAN-derived carbon fibres and resulting composites by active screen plasma surface functionalisation

Liang, Yana; Li, Xiaoying; Semitekolos, Dionysis ; Charitidis, Costas; Dong, Hanshan

DOI:
10.1002/ppap.201900252

Document Version
Publisher's PDF, also known as Version of record

Citation for published version (Harvard):
Liang, Y, Li, X, Semitekolos, D, Charitidis, C & Dong, H 2020, 'Enhanced properties of PAN-derived carbon fibres and resulting composites by active screen plasma surface functionalisation', *Plasma Processes and Polymers*, vol. 17, no. 4, 1900252. https://doi.org/10.1002/ppap.201900252

Received: 6 December 2019 | Revised: 27 January 2020 | Accepted: 2 February 2020

DOI: 10.1002/ppap.201900252

FULL PAPER

PLASMA PROCESSES AND POLYMERS

Enhanced properties of PAN-derived carbon fibres and resulting composites by active screen plasma surface functionalisation

Yana Liang[1] | **Xiaoying Li**[1] | **Dionisis Semitekolos**[2] | **Costas A. Charitidis**[2] | **Hanshan Dong**[1]

[1]School of Metallurgy and Materials, University of Birmingham, Birmingham, UK

[2]School of Chemical Engineering, National Technical University of Athens, Athens, Greece

Correspondence
Yana Liang, School of Metallurgy and Materials, University of Birmingham, Birmingham B15 2TT, UK.
Email: Y.Liang2019@outlook.com

Funding information
Horizon 2020 Framework Programme, Grant/Award Number: 685844; Engineering and Physical Sciences Research Council

Abstract

Advanced active screen plasma (ASP) technology is used to modify polyacrylonitrile-derived carbon fibre (CF) surfaces using gas mixtures of N_2–H_2 and N_2–H_2–Ar. Unlike conventional plasma treatments, ASP treatment can reduce the structural disorder of CF surfaces and increase the surface crystallite size. Moreover, ASP treatment can lead to an increased single fibre tensile strength. This is mainly because the post-plasma nature of the ASP technology can effectively eliminate ion-bombardment-induced degradation while providing radicals necessary for surface modification. The addition of argon to the nitrogen–hydrogen gas mixture contributes to a more ordered graphitic structure on CF surfaces and further increases the single fibre tensile strength. The interfacial properties (interlaminar shear strength and flexural strength) of the resulting composites are improved.

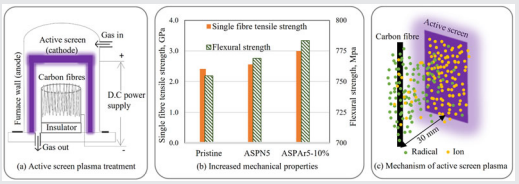

KEYWORDS
active screen plasma, carbon fibre, interfacial property, tensile strength

1 | INTRODUCTION

Carbon fibre (CF) acquires a pioneering position in structural applications due to its outstanding mechanical properties, high strength-to-weight ratio, and high thermal stability. Due to their high specific strength, CF-reinforced polymer composites are gradually replacing other conventional materials in automotive, civil construction, rail, aerospace, aviation and off-shore applications.[1,2] It is well-known that CFs are used as reinforcements in composites, provided the stress applied to the substrate can fully transfer to the CFs. However, because of the chemical inertness and low free energy of CF surfaces with high-density graphitic basal planes, the interfacial bonding is not strong enough to fully transfer the stress from the substrate to the CFs.[3] Therefore, further increase in the performance of CF-reinforced composites is restricted by the low CF/substrate interfacial shear strength.

Extensive research has been conducted on the physico-chemical interaction between CFs and the

matrix,[4–6] and a range of surface-engineering methods have been studied with the aim to enhance CF/substrate interfacial strength, such as chemical/electrochemical oxidation, plasma treatment, polymer grafting, sizing and nanoparticle coating.[3,7–12] All these techniques aim to modify the surface morphology of CFs, to introduce new chemical groups to the CF surface, and to change the surface free energy and hence improve the CF/matrix interfacial bonding. For instance, chemical oxidation generally etches the fibre surface and implants carbonyl and hydroxyl groups on the fibre surface, resulting in better bonding. However, it has been widely recognised that although chemical and electrochemical oxidation treatment can increase the fibre/matrix interfacial strength, the strength of the treated single fibre is significantly reduced mainly due to fibre surface damage.

Plasma treatment is highlighted as an environment-friendly, economic, and adaptable process for surface treatment of CFs with less impact on the fibre strength. However, conventional plasma still damages the fibre surface due to bombardment.[13] For example, Jang[14] reported that oxygen plasma treatment improved the fibre/matrix interfacial adhesion but at the cost of reduced average tensile strength from 3.80 to 3.01 GPa; ammonia gas plasma has a less damaging effect, but it still reduces the filament tensile strength from 3.80 to 3.65 GPa.

Recently, a more advanced plasma technology, active screen plasma (ASP), has been developed to avoid the undesirable effects associated with traditional direct plasma treatment, such as arcing, edge effects, and hollow-cathode damage.[15] This is because the cathode potential is applied to the active screen rather than to the samples to be treated and hence there is no direct ion bombardment to the sample surface during ASP treatment. Therefore, a feasibility study has been conducted by Gallo et al.[16] to explore the potential of ASP for the surface treatment of CFs. Although the preliminary work has revealed functionalised hydrophilic CF surfaces, it is not clear, if and how ASP treatment affects the strength of CFs.

In this study, the ASP technology has been utilised to systematically investigate the surface modification of polyacrylonitrile (PAN)-derived CFs using gas mixtures of nitrogen–hydrogen and nitrogen–hydrogen with different amounts (5–15%) of argon for varying treatment durations (2–8 min) to develop an optimal ASP treatment procedure for CFs. The modified CF surfaces were fully characterised by scanning electron microscopy (SEM), atomic force microscopy (AFM), X-ray diffraction (XRD) and Raman spectroscopy to understand the response of CFs to the ASP. Single fibre tensile tests were carried out to directly study the effect of ASP treatment on single fibre tensile strength; interlaminar shear strength (ILSS) and flexural strength of CF/epoxy composites were also measured.

2 | EXPERIMENTAL METHODS

2.1 | Materials

The CF used in this study was HTA40 E13 6K 400 tex provided by Toho Tenax®-E. It is a PAN-derived CF and commercially available as epoxy sized. The average diameter of this CF is approximately 7 μm, and typical tensile modulus and strength are about 238 and 3.9 GPa, respectively. 5H satin weave CF fabric G0926 was based on HTA40 with a typical density of around 370 g/m^2 and a thickness of 0.38 mm obtained from Hexcel Industries Inc. A three-part epoxy-based resin system (Araldite® LY556, Aradur® 917 and Accelerator® DY 070) was purchased from Huntsman industries and used as the matrix material.

2.2 | ASP treatments

ASP treatments were carried out at a pressure of 75 Pa in an AS Plasma Metal 75 kVA + 15kV industrial scale unit, which is equipped with an austenitic stainless steel mess cylinder as the active screen. The temperature within the furnace was measured by placing a thermocouple next to the samples. The voltage, controlled from 300 to 400 V, was applied between the active screen (cathode) and the wall of the furnace (anode) during all processes. The CFs were hung on a stainless steel rack with a distance of 30 mm to the active screen (Figure 1). The treatment current was recorded to be between 60 and 70 A, and the temperature in the furnace increased from room temperature (~25°C) to about 32°C for all treatments. As shown in Table 1, two groups of ASP treatments were designed to study the effect of gas mixtures and treatment durations. The first group of ASP treatments were conducted for 2, 5 and 8 min in a gas mixture of 25% N_2 and 75% H_2 (ASPN). The second group of ASP treatments were carried out for 5 min with 5–15% Ar in the gas mixtures (ASPAr).

2.3 | Surface analysis

SEM, JEOL 7000 and AFM (Innova, BRUKER) were used to observe the changes in the surface morphologies of CFs.

Raman spectra were obtained by using a Renishaw inVia Raman microscope. At least three spectra were recorded at different spots on the same sample. The raw

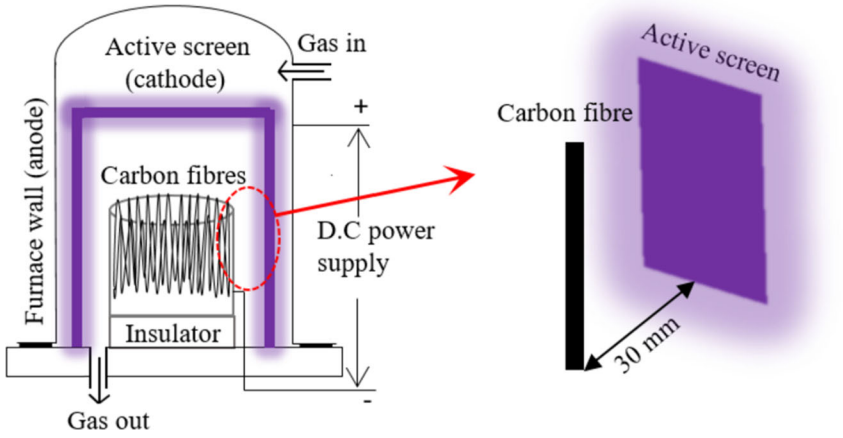

FIGURE 1 Schematic diagram of active screen plasma treatments

experimental data of the Raman spectra were peak-fitted by mixed Gaussian–Lorentzian curve to determine the peak intensities and Raman shifts.

XRD (Bruker D8) was employed to study the graphite-like crystal structure of the CFs before and after ASP treatments. The peaks of (002) and (10) were used to calculate the d_{002} spacing, the crystallite height *L*c and the crystallite width *L*a. The CF samples were grinded to powder by a cryomiller and then scanned from 10° to 90° at a speed of 10 s per step (0.01418°). The obtained XRD patterns were fitted with the Gaussian function to calculate the fibre structure parameters.

2.4 | Single fibre tensile strength tests

Single fibre tensile strength testing was performed using a universal testing machine Instron with a load cell of 10 N and a crosshead speed of 0.2 mm/min. Individual fibre was separated from fibre bundles carefully and each end was glued to a paper frame with a gauge of 25 ± 0.5 mm. The paper frame was gripped to the testing machine and was then cut into two parts before testing. The testing procedure was in accordance with ASTM D 3379-75, and at least 30 specimens were tested for each type of CFs. The Weibull distribution function was used to statistically evaluate the single-CF tensile strength and variations.

TABLE 1 Active screen plasma treatment conditions and the corresponding sample codes

Sample code	Gas mixture	Duration (min)
Pristine	None	None
ASPN2	25% N_2 + 75% H_2	2
ASPN5	25% N_2 + 75% H_2	5
ASPN8	25% N_2 + 75% H_2	8
ASPAr5-5%	5% Ar + 23.75% N_2 + 71.25% H_2	5
ASPAr5-10%	10% Ar + 22.5% N_2 + 67.5% H_2	5
ASPAr5-15%	15% Ar + 21.25% N_2 + 63.75% H_2	5

2.5 | ILSS and flexural strength

The interfacial interaction between the CF and the epoxy resin was estimated by the ILSS and flexural strength of the composite specimens. A composite panel was manufactured with the LY556 resin system by a vacuum infusion technique with eight piles of carbon fabrics (300× 300 mm) and then cut into specimens with the dimensions of 127 × 12.7 × 3.2 mm by a water jet CNC machine. The bending and shear stress were recorded by an analog compression force dynamometer (Tiedemann Instruments) according to ASTM D790 and ASTM D2344 standards, respectively. Bending and shear stress tests were repeated with five specimens. During the shear strength test, the composite specimens were broken into two segments, and the untouched fracture surface was observed by SEM with Jeol 6060.

3 | RESULTS AND DISCUSSION

3.1 | Results

3.1.1 | Surface morphology

The surface morphologies of the pristine and ASP-treated CFs observed by SEM are displayed in Figure 2. As expected, the surface of the pristine presented ridges and striations parallel to the fibre axial direction due to the PAN

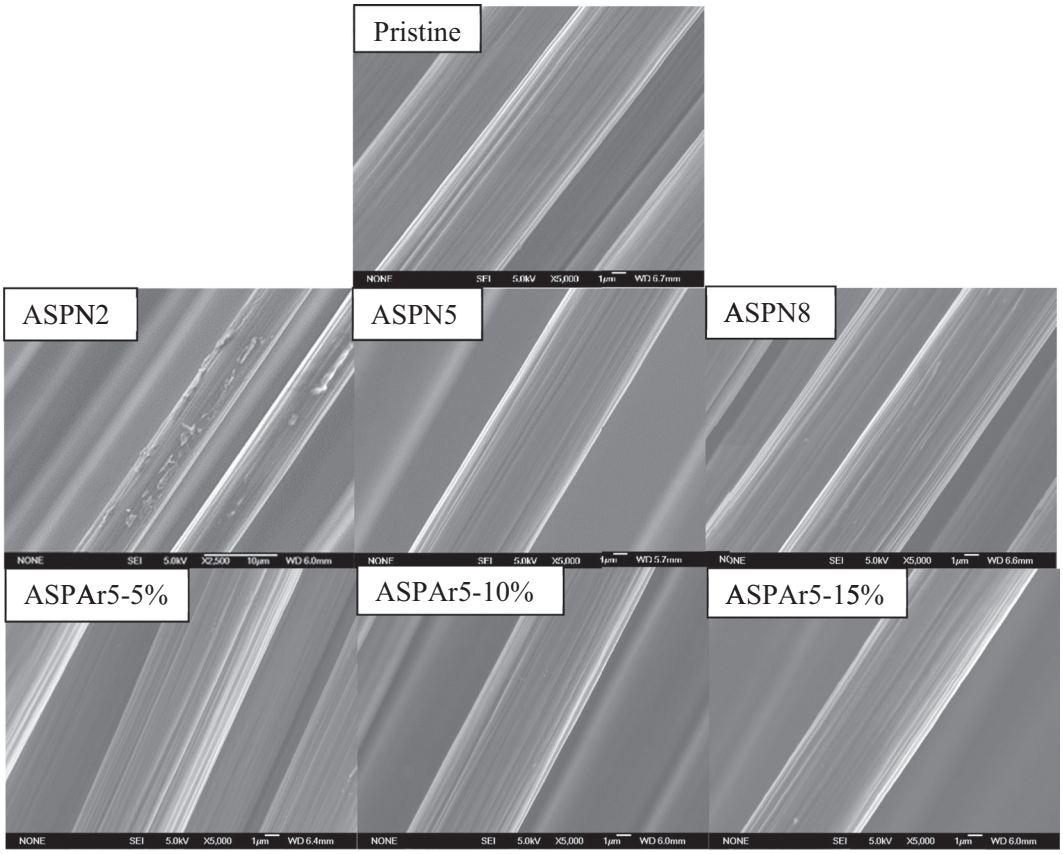

FIGURE 2 Carbon fibre surface morphologies observed by scanning electron microscopy

manufacturing process even though it was sized. It can be seen that after ASPN treatment for 2 min (ASN2), the most sizing coating material on the CFs were partially removed with some sizing patches remaining on the surface. After ASPN treatment for 5 min, no sizing patches could be observed under high-magnification (×5,000) SEM from the surface of the CFs (see ASPN5). No noticeable further changes could be clearly seen from the 8-min ASPN-treated CF surfaces (ASPN8) or all ASPAr-treated surfaces.

Further AFM analysis of the samples confirmed the above findings. The surface of the pristine CFs is fully covered by the sizing layer (Figure 3), while deep and wide grooves were revealed on the surface of the ASPN-treated samples with limited sizing patches remaining. However, the surfaces of ASPAr-plasma-treated samples showed dense and well-defined grooves with only very limited sizing traces. This indicates that the surfaces of the treated fibres are rougher than those of the pristine CFs and the plasma treatments with both nitrogen and argon (i.e., ASPAr) produced a stronger effect on the surface morphology change as compared with nitrogen alone (i.e., ASPN).

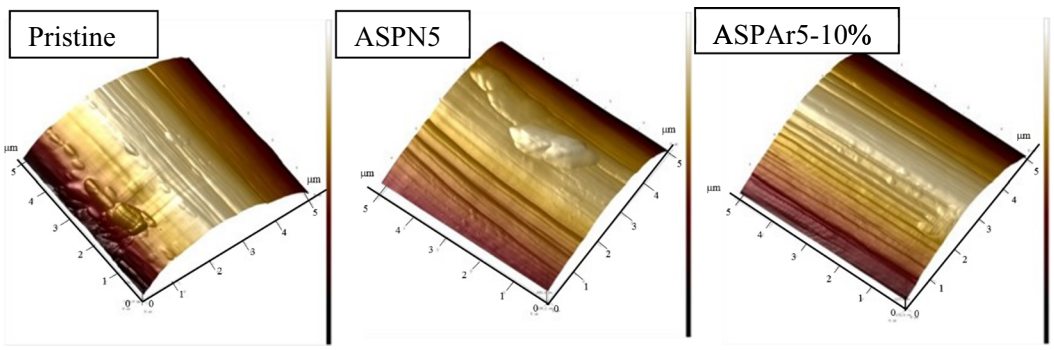

FIGURE 3 Carbon fibre surface morphologies observed by atomic force microscopy

3.1.2 | Distortion of CF surface after ASP treatments

Figure 4 presents the Raman spectra of the pristine and ASP-treated CFs. As a typical Raman spectrum described elsewhere, two broadening bands exhibited on all spectra are D band (disordered structure) and G band (ordered or graphitic structure). Both bands on the spectra of the ASPN-treated samples are similar to these bands on the pristine CF spectrum but sharper than bands on the ASPAr-treated samples. The relative band parameters are summarised in Table 2.

For the ASPN-treated CFs, in general, the position of the D band shifted to a higher wavenumber, and the full width at the half maximum (FWHM) of D band increased with increasing treatment time. The position and FWHM value for the 2 min treated samples (ASPN2) were almost identical to that of pristine CF. This is mainly because the surface of the CFs had not been fully cleaned within the first 2 min, which can be supported by the surface morphologies of ASPN2 shown in Figure 2. It can be also found from Table 2 that for longer (5 and 8 min) treated samples (ASPN5 and ASPN8), the D band shifted to a higher wavenumber, and its FWHM reduced with the treatment time. However, the position of the G band of short-time-treated ASPN2 CFs shifted to a slightly lower wavenumber. The intensity ratio (I_D/I_G) for ASPN5- and ASPN8-treated CFs was slightly increased or the same, respectively, relative to that of the pristine CFs. However, the I_D/I_G ratio of the short-time ASPN-treated ASPN2 CFs was reduced to 1.002 from 1.014 for the pristine CFs.

No clear trend could be identified for the effect of ASPAr treatments on the position and FWHM of the treated CFs. However, all the I_D/I_G values for the ASPAr-treated fibres were smaller than that of the pristine CFs and followed a decreasing trend.

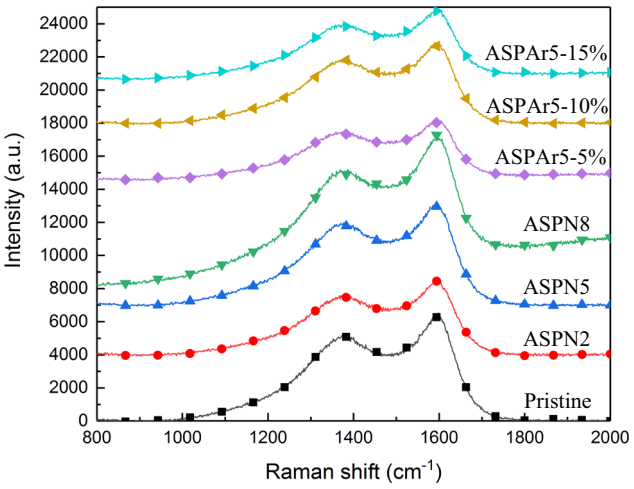

FIGURE 4 Raman spectra of pristine and active screen plasma treated carbon fibres

3.1.3 | Change of CF turbostratic structure by ASP treatments

The XRD diffraction patterns of pristine, ASPN5 and ASPAr5-10% are shown in Figure 5. The (002) peak for all samples is at approximately 24.6° (Reference code: 00-041-1487), which reflects the pseudographitic structure of CFs, and all the (002) peaks are very broad, indicating the presence of a certain amount of disorder in their structure. The peak (100) shown on pristine CFs faded away and overlapped with peak (101) on the XRD patterns of the treated samples. Thus, peaks (100) and (101) were integrated as (10) in this study to investigate the phase changes. Peaks (103), (110) and (112) at around 64.8°, 77.2° and 83.2° respectively, became sharper after both treatments. This phenomenon again implies that a certain amount of disorder was created by ASP treatments.

The 2θ peak width for peaks (002) and (10), crystal size parameter Lc (crystallite height) and La (crystallite width) are listed in Table 3. Lc and La were calculated from the parameters of the Gaussian-fitted peaks (002) and (10) with Scherrer's formula:

$$L = K\lambda/(\beta\cos\theta), \tag{1}$$

where K is a dimensionless shape factor ($Kc = 0.89$, $Ka = 1.84$); λ is the X-ray wavelength; β is the full peak width at the half maximum (FWHM); and θ is the Bragg angle of the corresponding peak.

It can be seen from Table 3 that the FWHM value for peak (002) decreased slightly for both treatments from 6.09 nm for pristine CFs to 5.83 nm for ASPN5 and 6.02 nm for ASPAr5-10%. The fading away of the peak (100) of the treated samples made the FWHM values of peak (10) much smaller than that of the pristine CFs. Both crystallite height Lc and width La increased for the treated CFs and more growth occurred in the crystallite width La. For example, the increase in La was more than 30 and 23 times to that in Lc for the ASPN5- and ASPAr5-10%-treated samples. The ratio of La/Lc increased from 2.99 for the pristine CFs to 4.21 and 3.29 for the ASPN- and ASPAr-treated CFs, respectively. This indicated that distorted microstructures with a significantly increased crystallite size were formed on the CF surface after the activation process and that more distortion happened along the basal planes for both treated samples.

3.1.4 | Tensile strength of single fibres

The Weibull plots and the fitted straight lines for the tensile-tested single fibres are presented in Figure 6 and

TABLE 2 Positions and FWHM of the D and G bands and the corresponding I_D/I_G ratio

	D band		G band		
Sample code	**Positions (cm^{-1})**	**FWHM (cm^{-1})**	**Positions (cm^{-1})**	**FWHM (cm^{-1})**	**I_D/I_G**
Pristine	1,392.9 (± 0.59)	289.7 (± 2.21)	1,595.2 (± 0.20)	105.3 (± 0.39)	1.014 (± 0.0179)
ASPN2	1,392.5 (± 0.79)	289.3 (± 1.73)	1,595.0 (± 0.29)	104.7 (± 0.46)	1.002 (± 0.0002)
ASPN5	1,394.6 (± 3.06)	296.7 (± 3.68)	1,595.5 (± 1.70)	104.8 (± 0.84)	1.018 (± 0.01273)
ASPN8	1,395.0 (± 1.04)	295.1 (± 3.92)	1,595.6 (± 0.64)	103.7 (± 0.78)	1.014 (± 0.0068)
ASPAr5-5%	1,389.5 (± 0.88)	285.5 (± 1.30)	1,594.2 (± 0.80)	104.7 (± 0.47)	1.009 (± 0.0149)
ASPAr5-10%	1,392.9 (± 0.96)	289.3 (± 3.62)	1,594.6 (± 0.33)	105.6 (± 0.94)	1.005 (± 0.0135)
ASPAr5-15%	1,390.3 (± 1.49)	293.5 (± 2.12)	1,594.5 (± 0.08)	104.2 (± 0.08)	1.004 (± 0.0078)

Note: Standard deviations given in brackets.
Abbreviation: FWHM, full width at the half maximum.

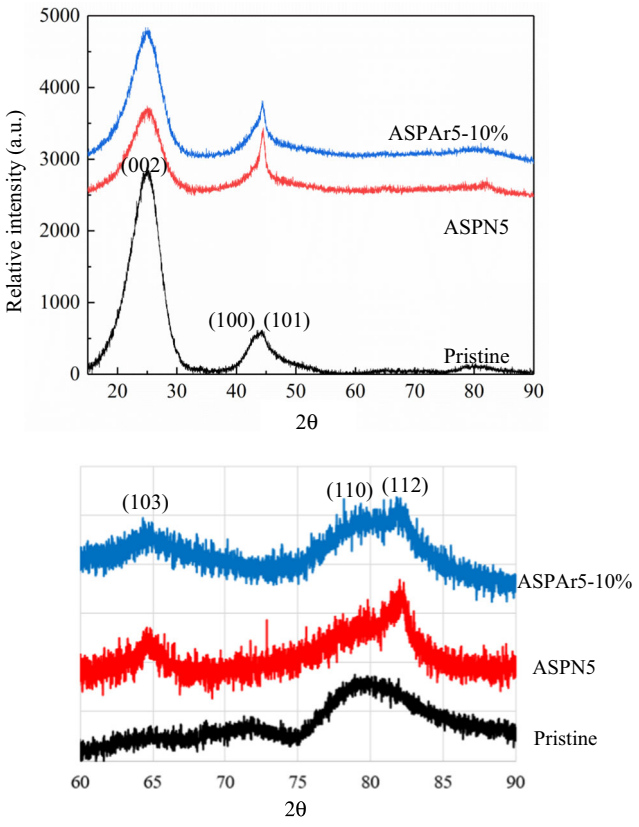

FIGURE 5 X-ray diffraction patterns of pristine, ASPN5 and ASPAr5-10% carbon fibres

the results of the Weibull statistical analysis for all the samples are summarised in Table 4. It can be seen that the Weibull plots were approximately linear, and all the fitting coefficient values R^2 are over 92%, signifying that the tensile strength of all CFs followed a Weibull distribution. The shape parameter m (or Weibull modulus) indicates the slope of the fitted lines and denotes the scattering of the single fibre tensile strength. The value of m decreased after all ASPN treatments, in which ASPN8 showed the greatest reduction. For the ASPAr-treated CFs, while ASPAr5-10%-treated CFs showed similar m value as the pristine CFs, the m value for other ASPAr-treated CFs was increased when compared with the pristine sample.

Compared with pristine CFs, the tensile strength of the ASPN-treated CFs increased before the treatment was prolonged to 8 min. This could be attributed to the change in the surface turbostratic structure and increased crystalline components. While prolonged plasma exposure could introduce surface defects, thus leading to a lower tensile strength.

The tensile strength of all ASPAr-treated CFs increased compared with the pristine CFs. Experiment with 5% of argon in gas mixture produced the most promising increase in tensile strength. Further increase in the argon percentage did not increase the strength further. It is also clear that the tensile strength of the ASPAr-treated CFs is higher than that of ASPN-treated ones. This should be attributed to the addition of argon to the gas mixture.

TABLE 3 XRD structure parameters

	Peak (002)			Peak (10)			
Sample code	**2θ (degree)**	**FWHM (nm)**	***Lc* (nm)**	**2θ (degree)**	**FWHM (nm)**	***La* (nm)**	***La*/*Lc***
Pristine	24.60 (± 0.011)	6.09 (± 0.027)	1.32	43.98 (± 0.054)	4.44 (± 0.131)	3.95	2.99
ASPN5	24.72 (± 0.017)	5.83 (± 0.042)	1.38	44.19 (± 0.024)	3.01 (± 0.058)	5.82	4.21
ASPAr5-10%	24.65 (± 0.010)	6.02 (± 0.024)	1.34	44.12 (± 0.027)	3.98 (± 0.065)	4.41	3.29

Note: Standard deviations given in brackets.
Abbreviations: FWHM, full width at the half maximum; XRD, X-ray diffraction.

3.1.5 | ILSS and flexural strength

The ILSS and flexural strength results are demonstrated in Figure 7. It is obvious that both the average flexural strength and ILSS increased after both ASPN and ASPAr treatments. The flexural strength increased from 754.6 MPa of the pristi6ne samples to 769.0 MPa for the ASPN-treated ASPN5 sample and 783.4 MPa for the ASPAr-treated ASPNAr5-10% sample. The pristine specimens revealed an ILSS of 43.7 MPa whereas the ASPN- and ASPAr-treated specimens revealed an ILSS of 46.4 and 43.9 MPa, respectively.

Moreover, the interlaminar shear fracture morphology along the cross-section of composites presented in Figure 8 also revealed that ASP treatment was able to improve the interfacial adhesion between the fibres and the resin. As shown in Figure 8, pristine CFs seemed to be separated from the matrix. There were few resin matrix adhered on the pristine CF surfaces and the CFs were pulled out of the composites. While for the samples reinforced by modified CFs, it is clear that the fibres and the matrix are bonded to each other tightly. The fracture surface seems relatively flat and the CFs were engulfed by matrix. These results further imply that the interfacial bonding between the CFs and the epoxy resin was improved after the ASP treatments.

3.2 | Discussion

3.2.1 | Increased strength of ASP-treated CFs

Plasma treatments have been reported to modify CF surfaces and hence to improve the CFs/matrix bonding in the resulting composites. Though, these plasma treatments can damage the fibre surfaces due to ion bombardment, leading to a reduction in the single fibre strength.[14,17] As exemplified in Figure 9 and reported by Sharma et al., plasma treatments significantly decreased the tensile load taken by the CFs before failure compared with the untreated CFs.

In contrast, as has been reported in Section 3.1.4, the tensile strength of ASP-modified CFs is higher than that of pristine CFs with an exception of ASPN8 (Table 4). The seemingly contradictory results could be attributed to the nature of the ASP used in this study, the interaction between the CF surfaces and the ASP and the resulting surface structure.

As can be seen from Figure 9, the reduction in the tensile property of CFs after conventional plasma treatments is accompanied with the increase in the structural disorder ratio (I_D/I_G) and the decrease in surface crystallite size *La*. However, for the ASP-treated CFs, the I_D/I_G intensity ratio decreased (except for ASPN5) and both the crystallite height *Lc* and width *La* increased with regard to that of the pristine CFs in this study. The correlation among the single fibre strength, structural disorder ratio (I_D/I_G) and surface crystallite size is valid for the ASP-treated CFs; although, the effect of plasma treatment on single fibre strength is opposite.

This is because during plasma treatments, the interactions between the sample and the plasma (ions, electrons and radicals) can lead to the functionalisation reactions and degradation reactions on the sample surfaces.[18–20] The functionalisation reactions are mainly initiated by the interaction with radicals, and the degradation reactions related to the etching effect are mainly initiated by the bombardment of ions.[21,22] Therefore, for most conventional direct plasma treatment (i.e., samples are immersed in plasma), increased fibre/matrix bonding promoted by the functionalisation reactions is at the cost of reduced single fibre strength due to the ion-bombardment-induced degradation reactions.

However, during the ASP treatments, the samples were placed about 30 mm away from the active screen where the plasma was generated. In essence, ASP treatment is a remote plasma or post-plasma treatment.[23,24] As a result, the radicals acted as the predominant

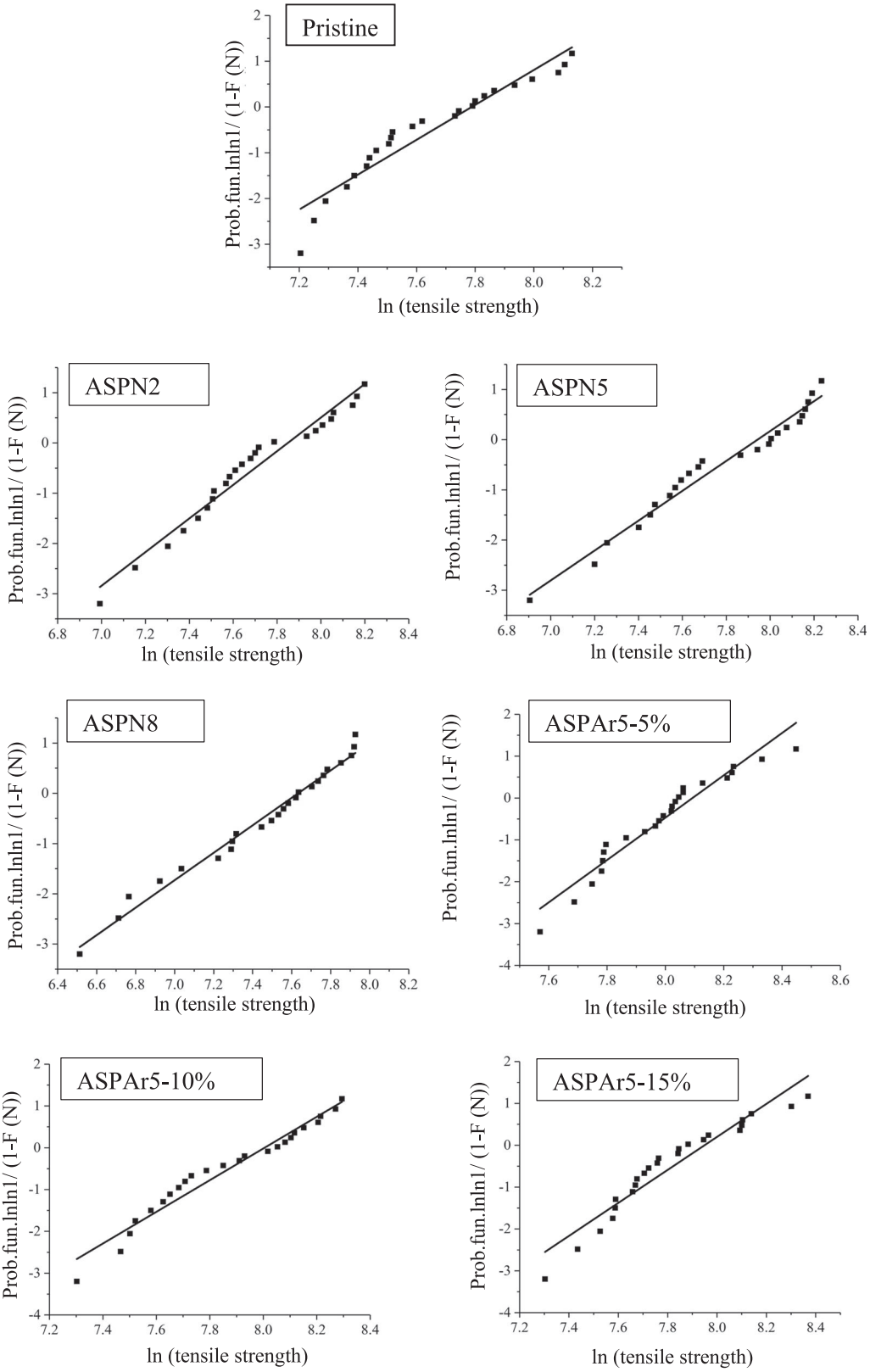

FIGURE 6 Weibull plots and linear fits for all groups of carbon fibres

component in the ASP and the ions and electrons acted as minor components on the sample surfaces because of a large difference in lifetime.[25] Accordingly, while radicals can easily reach CF surfaces for the desirable functionalisation reactions, a limited number of ions could bombard the CF surfaces, thus avoiding or reducing the undesirable degradation reactions. In other words, ASP treatment has the capability to separate the

TABLE 4 Summary of results from the Weibull analysis of single fibre tensile tests

Sample code	Intercept	Slope (m)	δ_0 (GPa)	R^2
Pristine	-29.70 ± 1.85	3.81 ± 0.24	2.41	0.92
ASPN2	-23.64 ± 0.84	2.98 ± 0.11	2.81	0.97
ASPN5	-26.27 ± 1.06	3.35 ± 0.14	2.56	0.96
ASPN8	-20.85 ± 0.58	2.73 ± 0.08	2.07	0.98
ASPAr5-5%	-40.93 ± 2.25	5.06 ± 0.28	3.27	0.94
ASPAr5-10%	-30.33 ± 1.31	3.79 ± 0.17	3.00	0.96
ASPAr5-15%	-31.34 ± 1.94	3.94 ± 0.25	2.83	0.92

radicals from ions and electrons to functionalise the CF surface, resulting in a decreased structural disorder (I_D/I_G) and an increased surface crystallite width (La).

These changes in the turbostratic structure could align the pseudocrystals with respect to the fibre axis, leading to a higher tensile strength.[26] In contrast, although the degradation reactions still exist during the ASP surface functionalisation process, the bombardment of the ions can be eliminated or reduced compared with the conventional plasma treatments due to the reduced number of ions that could reach the CF surfaces. This limited bombardment is beneficial to minimise the etching effect but still to remove the weakly bonded regions on the CF surfaces, which contributes to clean the surfaces and diminish critical sized flaws that act as stress concentrators. This is the main reason for the tensile strength increase of ASPN2. However, prolonged ASP treatment still increases the potential of degradation reactions and reduction of CF strength due to the accumulated ion bombardments on the CF surface, as evidenced by the decreasing strength of ASPN8. The degradation reactions can be indicated by the widening of D band for ASPN8, suggesting that defects or edge planes were created at the surface of the CFs by prolonged ASP treatments.

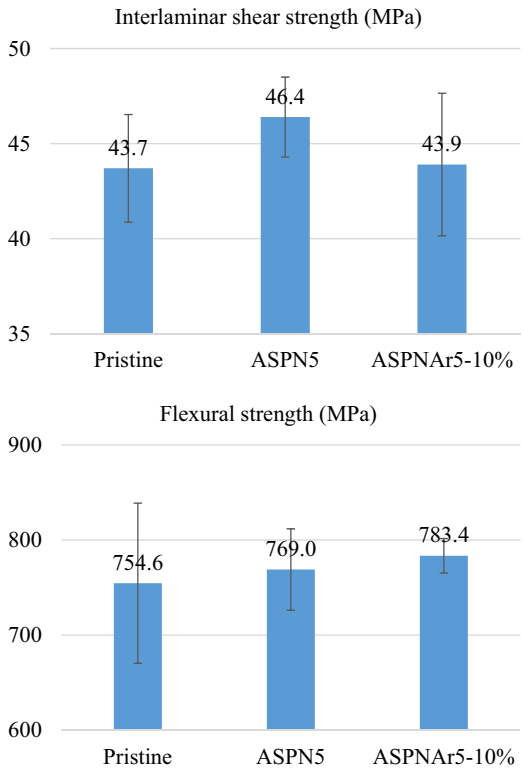

FIGURE 7 Interfacial shear strength and flexural strength of carbon fabric/epoxy resin composites

3.2.2 | Effect of Ar addition

As has been reported in Section 3.1, the addition of a small amount of argon into the ASP treatments produced a remarkable effect on the disordered microstructure and the tensile strength of the ASPAr-treated CFs as compared with that of the ASPN-treated one. As shown in Table 2, compared with the ASPN treatment, the ASPAr treatments showed less influence on the position and width of D band, which is an indication of the reduced degradation reactions. Moreover, the I_D/I_G intensity ratio decreased gradually with increasing argon concentration in the gas mixtures. As summarised in Table 3, the crystallite width La as well as the La/Lc decreased with the introduction of argon into the gas mixture.

These changes could be attributed to the difference in mean free path of argon, nitrogen and hydrogen species. According to the mean free path equation[27]:

$$\lambda_i = \frac{k_B T}{\sqrt{2}\pi p d^2}, \tag{2}$$

where k_B is Boltzmann constant, T is temperature, p is pressure and d is the diameter. As can be seen from the Table 5, the diameters of argon species are greater than those of the nitrogen and hydrogen species, which means that the argon species have a shorter mean free path compared with nitrogen and hydrogen species. As a result, the ion concentration around the CFs away from the active screen is lower during the ASPAr treatments than during the ASPN treatments. That is to say, when nitrogen/hydrogen is partially replaced by argon during the ASPAr treatments, the ion-etching-induced degradation effect can be reduced due to the reduced ion bombardments. Accordingly, the single fibre tensile strength is higher than that of the ASPN-treated CFs (Table 4).

However, the functionalisation reactions conferred by the radicals of argon, nitrogen and hydrogen still occurred

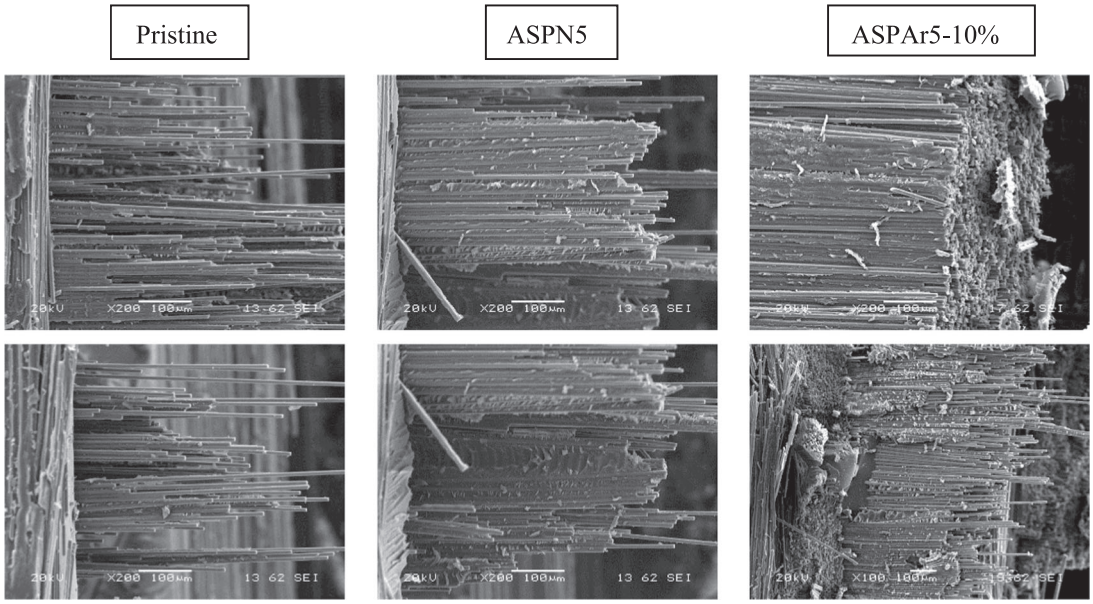

FIGURE 8 SEM side-view images of fracture surfaces

and even had a powerful impact on the CF structures, as evidenced by the decreased I_D/I_G intensity ratio as shown in (Table 2) and the decreased value of *La*/*Lc* (Table 3) relative to that of ASPN-treated CFs. This indicates that a more ordered graphitic structure and hence improved tensile strength have been achieved with the addition of argon in the ASPN treatments (i.e., ASPAr). However, the tensile strength of the ASPAr-treated CFs decreased by further increasing the argon concentration in the gas mixture. This could be attributed to the increasing number of radicals in the plasma, which possess a short mean free path, thus failing to functionalise the CF surfaces.

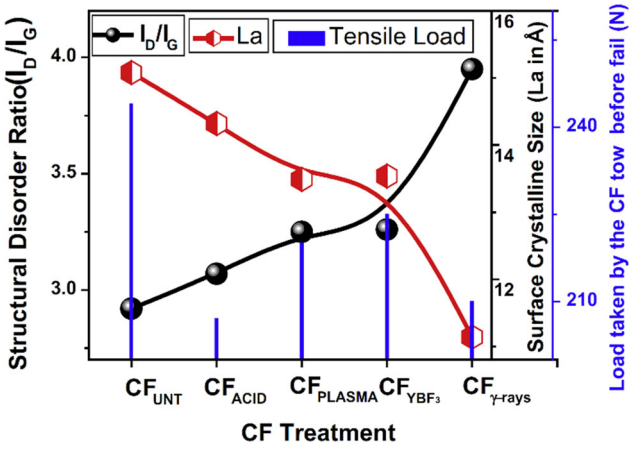

FIGURE 9 Variation of structural disorder parameter I_D/I_G, surface crystalline size *La* and tensile load of CFs as a function of various CF treatments. CF, carbon fibre; UNT, untreated; YBF_3, nano-ytterbium fluoride particles treated[7]

4 | SUMMARY AND CONCLUSIONS

ASP technology has been applied to modify the PAN-derived CF surfaces using gas mixtures of N_2–H_2 (ASPN) and N_2–H_2–Ar (ASPAr). The ASP treatments have successfully improved the ILSS and flexural strength of the resulting CF/epoxy composites. This implies that the ASP treatment can activate CF surfaces and enhance the CF/epoxy interfacial strength.

Unlike other conventional plasma treatments, advanced ASP treatment can lead to increased (rather than decreased, for other plasma treatments) single fibre tensile strength. This is mainly because the post-plasma nature of the ASP technology can effectively eliminate ion-bombardment-induced degradation while providing radicals necessary for surface modification as radicals have a longer lifetime than ions and electrons.

The introduction of argon in the nitrogen–hydrogen ASP (i.e., ASPAr treatment) can produce a more ordered graphitic structure on CF surfaces and further increase single fibre tensile strength compared with ASPN

TABLE 5 The atomic diameter and ionic diameter of H, N and Ar elements[28]

Element symbol	Atomic diameter (Å)	Ionic diameter (Å)
H	1.06	0.50
N	1.12	1.30
Ar	1.42	1.42

treatments due to the shorter mean free path of argon ions compared with that of nitrogen ions as the former has a larger diameter than the latter.

ACKNOWLEDGEMENTS

One of the authors (Y. L.) would like to appreciate the financial support from the Centre for Doctoral Training in Innovative Metal Processing (IMPaCT) funded by the UK EPSRC (EP/L016206/1). The research leading to these results has received funding from European Union's Horizon 2020 Research and Innovation Programme under grant agreement No. 685844. We would like to thank Craig Jones from THE WELDING INSTITUTE, UK for sharing AFM pictures shown in Figure 3.

ORCID

Yana Liang http://orcid.org/0000-0002-7187-9409

REFERENCES

[1] D. Akbar, Ü. E. Güngör, *Surf. Coat. Technol.* **2014**, *240*, 233.
[2] S. Tiwari, J. Bijwe, *Procedia Technol.* **2014**, *14*, 505.
[3] F. Severini, L. Formaro, M. Pegoraro, L. Posca, *Carbon* **2002**, *40*, 735.
[4] J. Schultz, L. Lavielle, C. Martin, *J. Adhes.* **1987**, *23*, 45.
[5] L. Shang, M. Zhang, L. Liu, L. Xiao, M. Li, Y. Ao, *Surf. Interface Anal.* **2019**, *51*, 199.
[6] J. Zhuoda, *Surf. Interface Anal.* **2019**, *51*, 458.
[7] M. Sharma, S. L. Gao, E. Mader, H. Sharma, L. Y. Wei, J. Bijwe, *Compos. Sci. Technol.* **2014**, *102*, 35.
[8] S. Corujeira Gallo, X. Li, K. Futterer, C. A. Charitidis, H. Dong, *ACS Appl. Mater. Interfaces* **2017**, *9*, 23195.
[9] D. Semitekolos, P. Goulis, D. Batsouli, E. P. Koumoulos, L. Zoumpoulakis, C. A. Charitidis, *Int. J. Struct. Integr.* **2019**, https://doi.org/10.1108/IJSI-08-2018-0050
[10] Z. Chen, X. J. Dai, P. R. Lamb, J. du Plessis, D. R. de Celis Leal, K. Magniez, B. L. Fox, X. Wang, *Plasma Processes Polym.* **2013**, *10*, 1100.
[11] Z. Dai, F. Shi, B. Zhang, M. Li, Z. Zhang, *Appl. Surf. Sci.* **2011**, *257*, 6980.
[12] R. M. Santos, D. Vale, J. Rocha, C. Martins, S. T. Mould, N. Rocha, *Fatigue Fract. Eng. Mater. Struct.* **2019**, *42*, 1521.
[13] L. Altay, E. Bozaci, M. Atagur, K. Sever, G. S. Tantug, M. Sarikanat, Y. Seki, *J. Appl. Polym. Sci.* **2018**, *136*, 47131.
[14] B. Z. Jang, *Compos. Sci. Technol.* **1992**, *44*, 333.
[15] X. Fu, M. J. Jenkins, G. Sun, I. Bertoti, H. Dong, *Surf. Coat. Technol.* **2012**, *206*, 4799.
[16] S. Corujeira Gallo, C. Charitidis, H. Dong, *J. Vac. Sci. Technol., A* **2017**, *35*, 021404.
[17] M. J. Sun, B. R. Hu, Y. S. Wu, Y. Tang, W. Q. Huang, Y. X. Da, *Compos. Sci. Technol.* **1989**, *34*, 353.
[18] N. Inagaki, *Plasma Surface Modification and Plasma Polymerization*, CRC Press, Boca Raton, FL **2014**.
[19] E. N. Voronina, A. A. Sycheva, D. V. Lopaev, T. V. Rakhimova, A. T. Rakhimov, O. V. Proshina, D. G. Voloshin, S. M. Zyryanov, A. I. Zotovich, Y. A. Mankelevich, *Plasma Processes Polym.* **2019**, https://doi.org/10.1002/ppap.201900165
[20] N. Peltekis, M. Mausser, S. Kumar, N. McEvoy, C. Murray, G. S. Duesberg, *Chem. Vap. Deposition* **2012**, *18*, 17.
[21] N. Inagaki, *Macromol. Symp.* **2000**, *159*, 151.
[22] M. M. Giangregorio, G. V. Bianco, P. Capezzuto, G. Bruno, M. Losurdo, *Plasma Processes Polym.* **2016**, *13*, 147.
[23] T. Desmet, T. Billiet, E. Berneel, R. Cornelissen, D. Schaubroeck, E. Schacht, P. Dubruel, *Macromol. Biosci.* **2010**, *10*, 1484.
[24] K. Fairbairn, H. K. Ponnekanti, D. Cheung, T. Tanaka, M. Kelka (Applied Materials, Inc.), *U.S. Patent 5,844,195*, **1998**.
[25] E. E. Kunhardt, L. H. Luessen, *Electrical Breakdown and Discharges in Gases: Part A Fundamental Processes and Breakdown*, Springer Science & Business Media, Berlin, Germany **2013**.
[26] D. J. Johnson, *J. Phys. D: Appl. Phys.* **1987**, *20*, 286.
[27] S. Chapman, T. G. Cowling, D. Burnett, *The Mathematical Theory of Non-uniform Gases: An Account of the Kinetic Theory of Viscosity, Thermal Conduction and Diffusion in Gases*, Cambridge University Press, Cambridge, UK **1990**.
[28] Atomic radii, http://www.crystalmaker.com/support/tutorials/atomic-radii/. (accessed: January **2020**).

How to cite this article: Liang Y, Li X, Semitekolos D, Charitidis CA, Dong H. Enhanced properties of PAN-derived carbon fibres and resulting composites by active screen plasma surface functionalisation. *Plasma Process Polym*. 2020;17:e1900252. https://doi.org/10.1002/ppap.201900252